Proposal and testing of dual-beam dynamic light scattering for two-particle microrheology

Xin-Liang Qiu, Penger Tong, and Bruce J. Ackerson

A dual-beam dynamic light-scattering arrangement is devised to measure the time-dependent mean squared relative displacement of a pair of tracer particles with a small separation of micrometers. The technique is tested by the measurement of the relative diffusion of polymer latex spheres suspended in a simple viscous fluid. The experiment verifies the theory and demonstrates its applications. The dual-beam dynamic light-scattering technique, when combined with an optical microscope, provides a powerful tool for the study of two-particle microrheology of soft materials. The advantages of the new technique are its high statistical accuracy, faster temporal response, and ease of use. © 2004 Optical Society of America

OCIS codes: 120.5820, 290.5850, 300.6480.

1. Introduction

Of much fundamental interest in the study of microrheology of soft materials or complex fluids is the time-dependent mean squared displacement (MSD) of a tracer particle, $\langle \Delta \mathbf{r}^2(\tau) \rangle_t = \langle |\mathbf{r}(t + \tau) - \mathbf{r}(t)|^2 \rangle_t$, where $\mathbf{r}(t)$ is the position of the particle at time t, τ is the lag time, and the angle brackets $\langle \cdots \rangle_t$ indicate an average over t. For particles suspended in a simple fluid of viscosity η, their MSD is determined by the Brownian diffusion by means of $\langle \Delta \mathbf{r}^2(\tau) \rangle_t = 6D_0\tau$, where $D_0 = k_B T/(6\pi\eta a)$ is the single-particle diffusion constant given by the Stokes–Einstein relation.[1] Here $k_B T$ is the thermal energy and a is the particle radius. In complex fluids exhibiting both viscous and elastic behavior, the Stokes–Einstein relation is generalized[2–5] to give

$$\langle \widetilde{\Delta \mathbf{r}}^2(s) \rangle = \frac{3k_B T}{\pi a s \tilde{G}(s)}, \tag{1}$$

where s is the Laplace frequency, $\langle \widetilde{\Delta \mathbf{r}}^2(s) \rangle$ is the Laplace transform of $\langle \Delta \mathbf{r}^2(\tau) \rangle$, and $\tilde{G}(s)$ is the projection of the frequency-dependent complex shear modulus $G^*(\omega)$ in the Laplace space. The real part of $G^*(\omega)$ is the elastic-storage modulus $G'(\omega)$ and the imaginary part is the viscous-loss modulus $G''(\omega)$.

With the generalized Stokes–Einstein relation (GSER), one can probe the viscoelastic properties of complex fluids by simply measuring the thermal motion of micrometer-sized tracer particles embedded in the material. Dynamic light scattering (DLS), diffusion wave spectroscopy, laser deflection particle tracking, and multiparticle tracking (MPT) with video microscopy have been used to measure the MSD of individual tracer particles in various complex fluids and biomaterials.[6–11] Other methods of measuring the one-particle MSD are cited in the recent reviews.[6–9] The one-particle microrheology offers two potential advantages over conventional rheometers. First, it provides a microscopic probe to study the local properties of rheologically inhomogeneous samples. Second, it requires only a minuscule sample volume, making the technique particularly useful for biological samples that are difficult to obtain in large quantities. To fully utilize these advantages, one needs to ensure that the tracer particles embedded in the sample are inert, so that they do not perturb the local environment of the material under study. Although one-particle microrheology provides an accurate measurement of $G^*(\omega)$ for simple systems, its validity in common complex systems is far from certain. The experimental situation is often complicated by the adsorption and depletion of macromolecules in the medium, electrostatic interactions, and other effects that are peculiar to the system under study.[12,13]

The authors are with the Department of Physics, Oklahoma State University, Stillwater, Oklahoma 74078. P. Tong is also with the Department of Physics, Hong Kong University of Science and Technology, Clear Water Bay, Kowloon, Hong Kong (e-mail, penger@ust.hk).

Received 15 July 2003; revised manuscript received 26 February 2004; accepted 4 March 2004.

0003-6935/04/173382-09$15.00/0

To overcome the experimental difficulties, Crocker *et al.*[13] recently developed two-particle microrheology, which measures the relative diffusion of tracer particle pairs within the sample. The correlated motion of the particle pairs depends only on the separation l between the particles and is independent of the particle size. This increase in length scale from the particle radius a to the particle separation l means that two-particle microrheology is insensitive to the sample inhomogeneities of sizes smaller than l and thus measures the true microrheological properties of the sample, even if one-particle microrheology does not. In two-particle microrheology, one is interested in the mean squared relative displacement (MSRD) of tracer particle pairs, $\langle \Delta \mathbf{r}_{21}{}^2(l, \tau)\rangle_t \equiv \langle |\mathbf{r}_{21}(t+\tau) - \mathbf{r}_{21}(t)|^2\rangle_t = \langle |\Delta \mathbf{r}_2(t, \tau) - \Delta \mathbf{r}_1(t, \tau)|^2\rangle_t$, where $\mathbf{r}_{21} = \mathbf{r}_2 - \mathbf{r}_1$ is the distance between the two particles and $\Delta \mathbf{r}_i$ is the displacement vector of the ith particle defined above. From this definition one finds that MSRD contains both the self-diffusion terms $\langle \Delta \mathbf{r}_i{}^2\rangle_t$ (single-particle MSD) and the cross-diffusion term $\langle \Delta \mathbf{r}_2 \cdot \Delta \mathbf{r}_1\rangle_t$. Because of the axial symmetry of the problem, the relative diffusion between the particles is no longer isotropic, and both the longitudinal and the transverse diffusion constants are needed to describe $\langle \Delta \mathbf{r}_2 \cdot \Delta \mathbf{r}_1\rangle_t$. It has been shown[4,5,13] that the GSER is still valid for $\langle \Delta \mathbf{r}_2 \cdot \Delta \mathbf{r}_1\rangle_t$, except that the particle radius a in Eq. (1) needs to be replaced with the particle separation l. In the experiment, Crocker *et al.*[13] used the MPT method together with video microscopy[14] to obtain $\langle \Delta \mathbf{r}_2 \cdot \Delta \mathbf{r}_1\rangle_t$.

In this paper we show that, with a two-incident-laser-beam arrangement and a new signal-processing scheme, DLS can be used to measure the relative motion between the tracer particles embedded in a viscoelastic medium. The dual-beam DLS technique, when combined with an optical microscope (hereafter referred as micro-DLS), provides a powerful tool for the study of two-particle microrheology of various soft materials. Compared with the video-based MPT methods, micro-DLS has the advantages of better averaging, higher accuracy, faster temporal response, and ease of use. It is a local probe that measures the relative motion of the particles in real time and is capable of mapping out the strain field in a rheologically inhomogeneous sample by using the scanning capability of the microscope stage.

The remainder of the paper is organized as follows. Section 2 contains the theoretical calculation of the intensity autocorrelation $g(\tau)$ in the two-beam arrangement. Experimental details appear in Section 3, and the results are presented and analyzed in Section 4. Finally, the work is summarized in Section 5.

2. Theory

We consider the scattering by N identical particles suspended in a dilute solution. Figure 1(a) shows the scattering geometry of the experiment. Two parallel laser beams with a small separation l are directed through the scattering sample. The frequency of one of the incident beams is shifted by Ω (=40 MHz). The polarization direction of the incident beams is perpendicular to the scattering plane, which is defined by the incident wave vector $\mathbf{k}_i$ and the scattered wave vector $\mathbf{k}_s$. The momentum-transfer vector is $\mathbf{q} = \mathbf{k}_s - \mathbf{k}_i$, and its amplitude is given by $q = (4\pi n/\lambda)\sin(\theta/2)$, where θ is the scattering angle, n is the refractive index of the solvent, and λ is the wavelength of the incident light. The photodetector records the scattered light intensity $I(t)$ by the particles with the same polarization and momentum-transfer vector $\mathbf{q}$ (i.e., at the same scattering angle θ) but from two spatially separated locations. The collected signals from the two regions (i.e., from two different particles with a separation l) interfere such that the resultant light $I(t)$ becomes modulated by Ω.

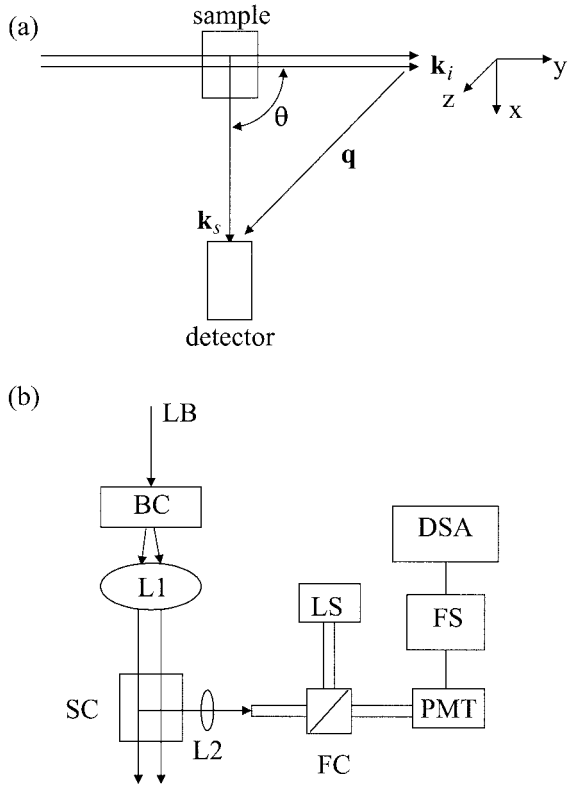

Fig. 1. (a) Schematic diagram of the scattering geometry (z axis is perpendicular to the paper): $\mathbf{k}_i$, incident wave vector; $\mathbf{k}_s$, scattered wave vector; θ, scattering angle; $\mathbf{q} = \mathbf{k}_s - \mathbf{k}_i$. (b) Schematic diagram of the experimental setup: LB, incident laser beam; BC, Bragg cell; L1, microscope objective; SC, sample cell; L2, collimating lens; FC, fiber-optic coupler; LS, He–Ne laser; PMT, photomultiplier tube; FS, frequency shifter; DSA, dynamical signal analyzer.

The intensity autocorrelation function $g(\tau)$ is written as

$$g(\tau) = \frac{\langle [E_1(t+\tau) + E_2(t+\tau)][E_1(t+\tau) + E_2(t+\tau)]^* [E_1(t) + E_2(t)][E_1(t) + E_2(t)]^* \rangle}{\langle [E_1(t) + E_2(t)][E_1(t) + E_2(t)]^* \rangle^2}, \quad (2)$$

where E_1 and E_2 represent the scattered electrical fields from each of the laser beams. The numerator on the right-hand side of Eq. (2) contains 16 terms.[15] Eight of these terms are of the form $\langle E_1E_2{}^*E_2E_2{}^*\rangle$ or $\langle E_2E_1{}^*E_1E_1{}^*\rangle$, with one field contributed from one scattering volume and three from the other. Because the particles that scatter the light are independently positioned in the two scattering volumes, the averaging over each volume may be carried out independently to obtain $\langle E_1\rangle\langle E_2{}^*E_2E_2{}^*\rangle$. Because a single field average $\langle E_1\rangle$ is zero, all eight of these terms may be neglected. There are two more zero-value terms of the form $\langle E_1{}^*(t+\tau)E_1{}^*(t)E_2(t+\tau)E_2(t)\rangle$ and $\langle E_1(t+\tau)E_1(t)E_2{}^*(t+\tau)E_2{}^*(t)\rangle$. These terms also separate into independent averages for each scattering volume, and the averages for each scattering volume are zero for the same reason that $\langle E_1\rangle$ is. Two other terms are time independent and are equal to $2I_1I_2$. Two of the remaining four terms are self-beat terms within each of the scattering volumes, $\langle I_1(t+\tau)I_1(t)\rangle$ and $\langle I_2(t+\tau)I_2(t)\rangle$. The last two terms are conjugated cross-beat terms, $\langle E_1{}^*(t+\tau)E_2(t+\tau)E_2{}^*(t)E_1(t)\rangle$ + c.c., which contain information about the hydrodynamic coupling between the two particles separated by distance l.

Equation (2) then becomes

$$\begin{aligned} g(\tau) &= 1 + \frac{{I_1}^2}{(I_1+I_2)^2}\,G_1(\tau) + \frac{{I_2}^2}{(I_1+I_2)^2}\,G_2(\tau) \\ &\quad + \frac{2I_1I_2}{(I_1+I_2)^2}\,G_{12}(\tau) \\ &\simeq 1 + bG_{12}(\tau), \end{aligned} \tag{3}$$

where $G_1(\tau) \propto \langle I_1(t+\tau)I_1(t)\rangle$ and $G_2(\tau) \propto \langle I_2(t+\tau)I_2(t)\rangle$ are two low-frequency self-beat terms, which will be filtered out in the experiment described below. The cross-beat correlation function, $G_{12}(\tau) \propto \langle E_1{}^*(t+\tau)E_2(t+\tau)E_2{}^*(t)E_1(t)\rangle$ + c.c., has the form

$$\begin{aligned} G_{12}(\tau) &= \frac{1}{N^2}\sum_{i,j}^{N}\langle\exp(i\mathbf{q}\cdot\{[\mathbf{r}_{2,i}(t+\tau) - \mathbf{r}_{1,j}(t+\tau)] \\ &\quad - [\mathbf{r}_{2,i}(t) - \mathbf{r}_{1,j}(t)]\} - i2\pi\Omega\tau)\rangle + \text{c.c.} \\ &= \langle\exp[i\mathbf{q}\cdot\Delta\mathbf{r}_{21}(\tau)]\rangle\cos(2\pi\Omega\tau), \end{aligned} \tag{4}$$

where $\mathbf{r}_{21} = \mathbf{r}_2 - \mathbf{r}_1$ is the distance between the two particles residing in the different scattering volumes and $\Delta\mathbf{r}_{21}(\tau) = \mathbf{r}_{21}(t+\tau) - \mathbf{r}_{21}(t)$ is the relative displacement vector of the two particles over the delay time τ. In deriving Eq. (4), we have assumed that the particles are uniformly distributed in the scattering volumes. Equation (4) states that $G_{12}(\tau)$ is an oscillatory function with its amplitude modulated by an ensemble-averaged phase factor $\langle\exp(i\mathbf{q}\cdot\Delta\mathbf{r}_{21})\rangle$ over all the particle pairs across the two scattering volumes.

For particles undergoing Brownian motion, their relative displacements are random and thus we have

$$\begin{aligned} \langle\exp[i\mathbf{q}\cdot\Delta\mathbf{r}_{21}(\tau)]\rangle &= \exp -\tfrac{1}{2}\langle[\mathbf{q}\cdot\Delta\mathbf{r}_{21}(\tau)]^2\rangle \\ &\simeq \exp -\tfrac{1}{2}k^2[\langle\Delta r_\parallel^2(l,\tau)\rangle \\ &\quad\times\langle(1-\cos\theta)^2\rangle \\ &\quad + \langle\Delta r_\perp^2(l,\tau)\rangle\langle\sin^2\theta\rangle]. \end{aligned} \tag{5}$$

In Eq. (5), $\Delta\mathbf{r}_{21}(\tau)$ is decomposed into two normal modes: $\Delta r_\parallel$ in the longitudinal direction parallel to $\mathbf{k}_s$ (and $\mathbf{r}_{21}$) and $\Delta r_\perp$ in the transverse direction perpendicular to $\mathbf{k}_s$ (in the scattering plane). In deriving the last relation of Eq. (5), we have used the facts that the ensemble average $\langle\Delta r_\parallel\Delta r_\perp\rangle = 0$ for random diffusion and the amplitudes of $\mathbf{k}_s$ and $\mathbf{k}_i$ are equal to $k = 2\pi n/\lambda$. In an ideal case, in which the photodetector sees only one pair of particles with $\mathbf{r}_{21}$ exactly parallel to $\mathbf{k}_s$ [i.e., when the length $\sigma_\parallel$ of the cylindrically shaped scattering volume (along the beam propagation direction) viewed by the photodetector is infinitesimally small], the angle θ in the last relation of Eq. (5) is simply the scattering angle shown in Fig. 1(a) and no average is needed for the weighting factors $(1-\cos\theta)^2$ and $\sin^2\theta$. In most experiments, however, the scattering volume viewed by a photodetector always has a finite length $\sigma_\parallel$ and thus the position vector $\mathbf{r}_{21}$ between the two particles has an angular spread $\theta \pm \delta\theta$ around $\mathbf{k}_s$. As a result, an average over the angular spread $\pm\delta\theta$ at a given scattering angle θ is needed for $(1-\cos\theta)^2$ and $\sin^2\theta$. We discuss details about the angular average in Section 4.

Equation (4) then becomes

$$\begin{aligned} G_{12}(\tau) &= \exp\{-\tfrac{1}{2}k^2[\langle\Delta r_\parallel^2(l,\tau)\rangle\langle(1-\cos\theta)^2\rangle \\ &\quad + \langle\Delta r_\perp^2(l,\tau)\rangle\langle\sin^2\theta\rangle]\}\cos(2\pi\Omega\tau). \end{aligned} \tag{6}$$

As mentioned in Section 1, the longitudinal and transverse components of the MSRD, $\langle\Delta r_\parallel^2(l,\tau)\rangle$ and $\langle\Delta r_\perp^2(l,\tau)\rangle$, contain both the self-diffusion contribution from $\langle\Delta\mathbf{r}_i{}^2\rangle_t$ and the cross-diffusion contribution from $\langle\Delta\mathbf{r}_2\cdot\Delta\mathbf{r}_1\rangle_t$. The self-diffusion contribution comes from the single-particle MSD and is independent of the particle separation l. Because the single-particle MSD is isotropic, the self-diffusion gives a common additive term to both $\langle\Delta r_\parallel^2(l,\tau)\rangle$ and $\langle\Delta r_\perp^2(l,\tau)\rangle$. As a result, the phase factor $\langle\exp(i\mathbf{q}\cdot\Delta\mathbf{r}_{21})\rangle$ in Eq. (4) becomes a product of two exponential functions: One is due to the self-diffusion and the other is due to the cross-diffusion, which depends on both l and τ. In two-particle microrheology, we are actually interested in the τ dependence of $\langle\Delta\mathbf{r}_2\cdot\Delta\mathbf{r}_1\rangle_t$, which is related to the complex shear modulus $G^*(\omega)$ by the GSER.[13] It is shown below that the decaying function that is due to the self-diffusion can be measured independently by use of the same experimental setup but with only one beam present in the scattering volume. Therefore the self-diffusion contribution can be readily divided out from the measured

$G_{12}(\tau)$ and the "corrected" $G_{12}(\tau)$ becomes the basic function for optical two-particle microrheology.

To further demonstrate the application of the technique, we now consider a simple system of uniform spheres suspended in a homogeneous viscous fluid (e.g., water). In this case, we have[16–19]

$$\langle \Delta r_{\parallel}^2(l, \tau)\rangle = 2D_{\parallel}\tau,$$
$$D_{\parallel} = 2D_0\left[1 - \frac{3a}{2l} + \mathbb{O}\left(\frac{a^3}{l^3}\right)\right], \qquad (7)$$

where $D_{\parallel}$ is the relative diffusion coefficient in the direction parallel to $\mathbf{k}_s$ (or $\mathbf{r}_{21}$) and D_0 is the single-particle free-diffusion constant. Similarly, we have

$$\langle \Delta r_{\perp}^2(l, \tau)\rangle = 2D_{\perp}\tau,$$
$$D_{\perp} = 2D_0\left[1 - \frac{3a}{4l} + \mathbb{O}\left(\frac{a^3}{l^3}\right)\right], \qquad (8)$$

for the relative diffusion in the direction perpendicular to $\mathbf{k}_s$ (or $\mathbf{r}_{21}$) in the scattering plane. It is seen from Eqs. (7) and (8) that both $D_{\parallel}$ and $D_{\perp}$ contain an l-independent term, $2D_0$, that is due to the self-diffusion contribution discussed above. Because the transfer of fluid into and out of the space between the two spheres is needed, the relative diffusion is suppressed compared with the free diffusion. This is especially true for $D_{\parallel}$. In this case, the relative motion between the two spheres must squeeze out of the fluid between them, producing extra resistance for the particle motion.

Substituting Eqs. (7) and (8) into Eq. (6), we have

$$G_{12}(\tau) = \exp\{-k^2[D_{\parallel}\langle(1 - \cos\theta)^2\rangle + D_{\perp}\langle\sin^2\theta\rangle]\tau\}\cos(2\pi\Omega\tau)$$
$$= \exp(-\tau/\tau_0)\cos(2\pi\Omega\tau), \qquad (9)$$

with

$$\tau_0 = \frac{1}{k^2[D_{\parallel}\langle(1 - \cos\theta)^2\rangle + D_{\perp}\langle\sin^2\theta\rangle]}$$
$$= \frac{t_0}{1 - \frac{3a}{4l}(1 + \langle\sin^2\theta/2\rangle)}. \qquad (10)$$

In Eq. (10), $t_0 = (2q^2D_0)^{-1}$ is the decay time in the absence of hydrodynamic coupling ($a/l \to 0$). It is also the decay time for the single-particle self-diffusion, which can be obtained independently by use of the usual one-beam DLS arrangement.[1] By measuring both the one-beam and two-beam correlation functions, we can divide out the self-diffusion contribution from the measured $G_{12}(\tau)$ in Eq. (9). In obtaining the last equality of Eq. (10), we have ignored the effect of the angular average over $\pm\delta\theta$ to the momentum-transfer vector $\mathbf{q}$. It has been shown[20] that such an average reduces the signal-to-noise ratio of the measured $g(\tau)$.

According to the Wiener–Khintchine theorem,[15] the frequency power spectrum $P(f)$ of the photocurrent is equal to the Fourier transform of $g(\tau)$. Therefore we have

$$P(f) = \frac{1}{2\pi}\int_{-\infty}^{\infty}\exp(i2\pi f\tau)G_{12}(\tau)\mathrm{d}\tau$$
$$\simeq \frac{1}{1 + (2\pi\tau_0)^2(f - \Omega)^2}. \qquad (11)$$

In the experiment, we can obtain τ_0 more accurately by plotting the measured $1/P(f)$ versus $(f - \Omega)^2$ and by fitting the data to a linear function:

$$1/P(f) = \alpha + \beta(f - \Omega)^2. \qquad (12)$$

From Eqs. (11) and (12), we obtain $\tau_0 = (\beta/\alpha)^{1/2}/2\pi$ from the two fitting parameters α and β.

3. Experiment

Figure 1(b) shows the experimental setup and optical arrangement. Incident laser beam LB from a solid-state laser (Coherent Verdi) of wavelength $\lambda = 532$ nm is directed through Bragg cell BC. The incident beam becomes multiple diverging beams when passing through the Bragg cell, which acts as an optical grating. In the experiment we use only the zeroth-order (unshifted) and the first-order (40-MHz shifted) outgoing beams, and all the higher-order beams are blocked. The Bragg cell is tilted slightly so that the two outgoing laser beams have equal intensity. A 100× microscope objective L1 is used to direct the two laser beams to sample cell SC. The distance between the objective and the beam-splitting point (inside the Bragg cell) is set to be equal to the focal length of the objective, such that the two outgoing beams become parallel at the measuring point. The sample cell is a square cuvette with dimensions 1 cm × 1 cm × 4 cm. It is filled with a dilute aqueous solution of uniform polymer latex spheres of radius a, which is varied from 0.07 to 0.95 μm. A long-working-distance telemicroscope (Leica MZ8, not shown) is used to view the incident laser beams directly from the top of the sample cell. Direct observation of the beam profile with the telemicroscope reveals that the two incident beams at the measuring point are separated by a distance $l = 10.5 \pm 1.5$ μm, which is fixed in the experiment.

The scattered light from the two parallel beams is collected by fiber-optic coupler FC, which consists of two input and two output single-mode fibers fused together. Only one input fiber is used in the experiment, and the light coming from the input fiber is evenly split into the two output fibers. A small collimating lens is installed at the front end of the input fiber for better collection of light. With the aid of extra collimating lens L2 ($f \simeq 2$ cm), the input fiber collects the light scattered by the particles with the same polarization and at the same scattering angle ($\theta = 90°$) but from two spatially separated beams. The two scattering spots viewed by the input fiber have a cylindrical shape of diameter $\sigma_{\perp} = 6.3 \pm 1.5$ μm and length (along the beam propagation direc-

tion) $\sigma_{\|} \simeq 12 \pm 2$ μm. The collected signals from the two regions (i.e., from two different particles separated by l) interfere such that the resultant light becomes modulated at the shift frequency $\Omega = 40$ MHz. This carrier frequency discriminates the self-beat signals (between the particles in the same incident beam) from the desired cross-beat signals between the particles across the two measuring volumes. Because Ω is much larger than the self-beat frequencies, we can readily remove the self-beat signals by using a high-pass filter.

One of the output fibers is connected to a photomultiplier tube (PMT), whose analog output is fed to frequency shifter FS (TSI Model 9186A). The frequency shifter is a phase-sensitive downmixer, which further shifts the 40-MHz optical carrier frequency down to a desired electronic carrier frequency Ω_0 in steps of 0, 2, 5, 10, and 20 kHz (other higher-frequency steps are not used in the experiment). The stability of the frequency shifter is better than 99.5%. The actual carrier frequency Ω_0 used for the output signals is chosen to obtain the highest frequency resolution possible. This signal is then fed to dynamical signal analyzer DSA (HP 35665A), which measures the intensity autocorrelation function $g(\tau)$ and the frequency power spectrum $P(f)$. In the measurement of $g(\tau)$, we choose $\Omega_0 = 0$. An oscilloscope is also connected to the output of the frequency shifter to view the signals directly. The frequency-shifting scheme allows us to measure low-frequency phase fluctuations accurately and at the same time filter out unwanted noise. The other output fiber is connected to He–Ne laser LS, which is used for optical alignment. With the reversed He–Ne light coming out of the input fiber, we can align the input fiber and directly observe the scattering volumes viewed by the PMT. The intersections between the output He–Ne beam and the two parallel incident beams define the scattering volumes. A beam stop is installed in the PMT housing to block the He–Ne light when the laser is on.

4. Results and Discussion

Figure 2 shows a typical trace of the scattered light intensity by particle pairs across the two scattering volumes. The signal is obtained directly from the analog output of the frequency shifter. It is seen that the signal has a carrier frequency of $\Omega_0 = 5$ kHz and its amplitude fluctuates at lower frequencies. To resolve the low-frequency fluctuations that are due to the Brownian motion of the particle pairs, we first set $\Omega_0 = 0$ and measure the intensity autocorrelation function $g(\tau)$. Figure 3 shows the measured $g(\tau) - 1$ as a function of delay time τ. The circles are obtained when two incident beams are used, and the squares are obtained when only one incident beam is present. We achieve this experimentally by simply turning on and off the Bragg cell.

As shown in Eqs. (9) and (10), $g(\tau) - 1$ becomes a simple exponential function when Ω is set at zero. (Experimentally, this is equivalent to setting $\Omega_0 = 0$.) The decay time of the measured $g(\tau) - 1$ is given by

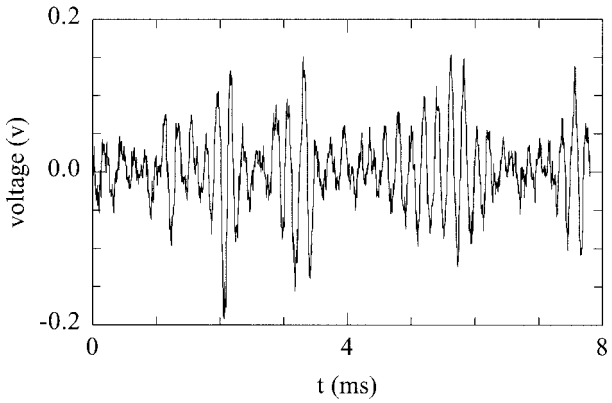

Fig. 2. Typical trace of the scattered light intensity across two scattering volumes separated by $l = 10.5$ μm. The particle size is 0.14 μm, and the electronic carrier frequency Ω_0 is 5 kHz.

$t_0 = 1/(2q^2D_0)$ for the one-beam arrangement and is increased by a factor of $1/[1 - (3a/4l)(1 + \langle \sin^2 \theta/2 \rangle)]$ when the two-beam arrangement is employed. These features are clearly shown in Fig. 3. The two-beam measurement shows a slower decay than does the one-beam measurement. The solid curves are the simple exponential fits to the data. We find that the difference in decay time between the two curves increases with the particle size. Evidently the hydrodynamic coupling between the particles increases with a/l.

To obtain the intensity autocorrelation function $g(\tau)$, the dynamical signal analyzer used in the experiment actually measures the frequency power spectrum $P(f)$ first and then Fourier transforms it back to $g(\tau)$. Figure 4(a) shows the $P(f)$ measured directly with $\Omega_0 = 0$. In this case, we obtain only a partial $P(f)$ for $f \geq 0$, because we cannot measure $P(f)$ at negative frequencies. In fact, we could also set the electronic carrier frequency Ω_0 to a value slightly larger than the characteristic frequency $1/t_0$ of the relative diffusion [see Eq. (10)] and obtain a full

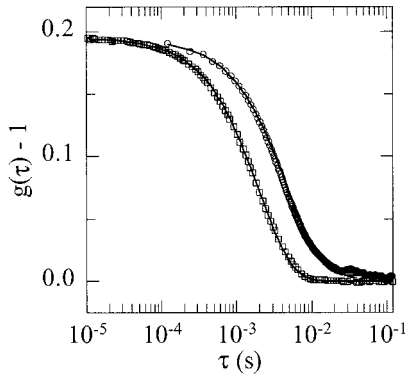

Fig. 3. Measured intensity autocorrelation function, $g(\tau) - 1$, as a function of delay time τ for particles of size 1.6 μm. The circles are obtained when two incident beams are used, and the squares are obtained when only one incident beam is present. The solid curves are the simple exponential fits to the corresponding data points.

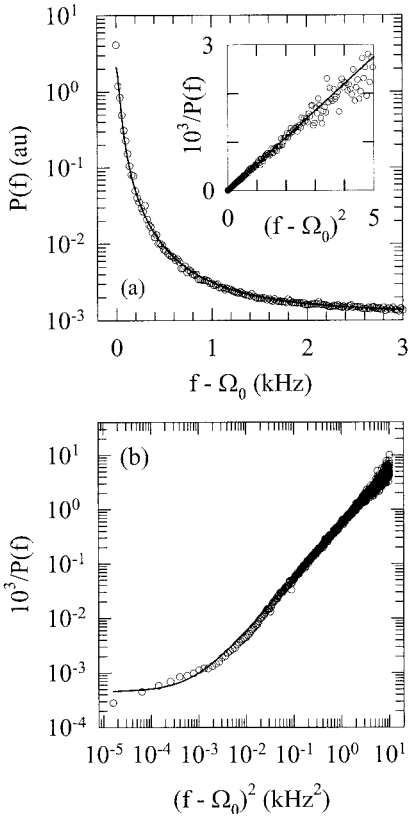

Fig. 4. (a) Measured frequency power spectrum $P(f)$ of the scattered light intensity when two incident beams are used (open circles). The solid curve is a fit to a Lorentzian function. In the measurement, Ω_0 is set to zero and the particle size is 1.6 μm. The inset shows a linear plot of $10^3/P(f)$ versus $(f - \Omega_0)^2$ for the same data set. (b) Corresponding log–log plot of $10^3/P(f)$ versus $(f - \Omega_0)^2$.

$P(f)$ for both $f < \Omega_0$ and $f \geq \Omega_0$. As shown in Eq. (11), the power spectrum $P(f)$ is a symmetric function of $f - \Omega_0$, and thus the measurement of a full $P(f)$ helps only in data averaging.

It is seen from Fig. 4(a) that the measured $P(f)$ decays slowly for more than three decades with a very small baseline (noise level). This is because the frequency-shifting scheme used in the experiment filters out most low-frequency noise. The measured $P(f)$ is well described by a Lorentzian function $P(f) = [\alpha + \beta(f - \Omega_0)^2]^{-1}$ (solid curve), where α and β are two fitting parameters. To determine the values of α and β more accurately, we plot $1/P(f)$ versus $(f - \Omega_0)^2$, as shown in the inset of Fig. 4(a). In this plot, α and β become, respectively, the intercept and the slope of a linear function. Note that the value of α is very small and is hard to see in the linear plot. To view α more clearly, we show a log–log plot of $1/P(f)$ versus $(f - \Omega_0)^2$ in Fig. 4(b). Using Eqs. (11) and (12) we obtain the decay time $\tau_0 = (\beta/\alpha)^{1/2}/2\pi$ from the fitted values of α and β. It is found that the value of τ_0 obtained from $P(f)$ agrees well with that obtained from $g(\tau)$.

Figure 5 compares the decay time obtained in the dual-beam arrangement (solid circles) with that obtained in the one-beam arrangement (open circles). As discussed in Section 2, the one-beam decay time is given by $t_0 = (2q^2D_0)^{-1}$ (dashed line), which is a linear function of the particle size $2a$. It is seen from Fig. 5 that the calculated t_0 is in good agreement with the one-beam measurements. The measured dual-beam decay time increases with $2a$ more rapidly, and thus the difference between the two sets of measurements, resulting from the cross-diffusion contribution, becomes larger for larger particles. As shown in Eq. (10), the effect of the hydrodynamic interaction between the particles increases with a/l (l is fixed in the experiment), and this is clearly seen in Fig. 5. For example, the two-beam measurement for particles of size 1.6 μm results in an ~45% increase in τ_0. For particles of size 0.14 μm, however, the two-beam measurement gives essentially the same result as does the one-beam measurement, indicating that the interparticle hydrodynamic coupling is negligible in this case.

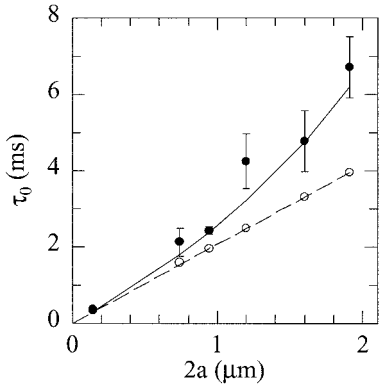

Fig. 5. Measured decay time τ_0 as a function of particle size $2a$. The solid circles are obtained when two incident beams are used. The open circles are obtained when only one incident beam is present. The solid curve is a fit to $\tau_0 = t_0/(1 - \gamma a/l)$, with $\gamma = 4 \pm 1$. The dashed line shows the one-beam decay time $t_0 = (2q^2D_0)^{-1}$.

The solid curve in Fig. 5 shows the fitted function $\tau_0 = t_0/(1 - \gamma a/l)$, with $\gamma = 4 \pm 1$. From Eq. (10), we expect $\gamma = (3/4)[1 + \langle \sin^2 \theta/2 \rangle] = (9/8)[1 - \langle \cos \theta \rangle/3]$. At the 90° scattering angle employed in the experiment, $\cos \theta$ is an odd function and its angular average over $\pi/2 \pm \delta\theta$ is zero ($\langle \cos \theta \rangle = 0$). Therefore we have $\gamma = 9/8$, which is approximately 3.6 times smaller than the fitted value. In deriving Eq. (10) we have assumed that all the particle pairs in the scattering volumes have the same separation l. Because of the finite size of each scattering volume, the actual separation of the particle pairs may vary in the range $l \pm \sigma_\perp$ (10.5 ± 6.3 μm). Such a variation in particle separation will give rise to a correction factor to the fitted γ. To calculate the correction factor, we need to know the intensity profile of each scattering volume.[21]

Another source of experimental error comes from the optical alignment. To focus the two incident laser beams in a small region, we used a 100× micro-

scope objective. Because of the tight focusing, the two laser beams become parallel to each other in only a very small waist region of size $\sigma_{\parallel} \simeq 12\ \mu m$. In this case, the detecting optics is required to have high accuracy in locating the proper scattering regions. Although we are able to detect the desired signals by using the convectional light-scattering apparatus, the overall optical arrangement used in the present experiment is not fully optimized. As shown in Fig. 5, the two-beam data have relatively larger error bars, which are estimated based on the scatterer of the measured MSRD values from run to run. The experimental uncertainties are largely related to the optical alignment. The use of strongly focused laser beams for illuminations introduces uncertainties for the momentum-transfer vector $\mathbf{q}$ and thus complicates the analysis of the scattering geometry.[20,22] This may also affect the final result for γ.

On the theoretical side, Hinch and Nitsche[23] proposed that the nonlinear hydrodynamic effect can lead to an additional mean force of interaction between two Brownian spheres, which may change the value of γ in Eq. (10). The calculation for the relative diffusion of particle pairs in Eqs. (7) and (8) uses the linear Stokes equation, and the nonlinear term is not included in the calculation. More accurate measurements are needed in order to test the theory by Hinch and Nitsche.

5. Proposal of Microdynamic Light Scattering

To overcome the experimental difficulties and further improve the accuracy of the dual-beam DLS for small samples, we herein devise a dual-beam DLS arrangement on an inverted microscope, which provides the best optics possible. Recently, Kaplan *et al*. have devised a one-beam DLS arrangement on an inverted microscope.[22] By the introduction of a coaxial laser beam along the optical axis of the microscope, the one-beam DLS collects the scattered light at the back focal plane (BFP) of the microscope objective. The collected signals from a point in the BFP have the same momentum-transfer vector $\mathbf{q}$. By use of an objective with a large numerical aperture, the one-beam DLS can measure $g(\tau)$ at a scattering angle θ up to $\sim 65°$, which is determined simply by the distance between the measuring point and the center of the BFP.

Figure 6 shows the optical arrangement for the dual-beam micro-DLS. This design is similar to that for the one-beam DLS[22,24] except that Bragg cell BC and collimating prism CP are added before lens L1, which is placed at a position conjugate to condenser CO. The two outgoing diverging beams from the Bragg cell, with one of the beams frequency shifted, become parallel after the collimating prism. The two parallel beams are further projected onto sample SA by both L1 and the condenser, which reduce the beam separation and diameter simultaneously by a factor proportional to the focal-length ratio between L1 and the condenser. In addition, a frequency shifter is used to process the electronic signals.

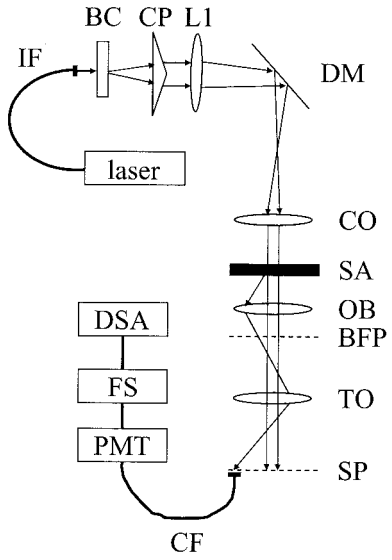

Fig. 6. Optical design of the dual-beam DLS microscope: IF, incident fiber; BC, Bragg cell; CP, collimating prism; L1, lens; DM, dichroic mirror; CO, condenser; SA, sample; OB, objective; BFP, back focal plane; TO, tube optics; SP, scattering plane; CF, collecting fiber; PMT, photomultiplier tube; FS, frequency shifter; DSA, dynamical signal analyzer.

This design has several new features. First, with the aid of the microscope we can directly view the two incident laser spots on the sample. The size of each spot can be reduced down to the diffraction limit ($\sim 0.2\ \mu m$) and the separation l between the two laser spots can be adjusted down to $\sim 1\ \mu m$. Using the microscope, we can also record the intensity profile of each laser spot with a CCD camera and carry out optical alignment in real time. Second, because the dual-beam DLS measures the relative displacement directly from the cross-beat signals, the accuracy of the two-particle MSRD measurement becomes as high as that of the one-particle MSD measurement made with the standard one-beam DLS. An alternative way of obtaining MSRD is to measure the position of individual particles separately and then get the difference between the particle positions by data subtraction. This is the approach employed by laser deflection particle tracking[3,10] and video-based MPT[11,13,16,19] methods. With these methods the measured MSRD may suffer large experimental uncertainties in certain cases in which the interparticle hydrodynamic coupling is weak and the signal is dominated by the uncorrelated motion. This is especially true when the particle motion is influenced by a large background noise that is due to vibration or velocity drifts.

Finally, the dual-beam micro-DLS uses a frequency-shifting scheme, which selects the right particle pairs and measures their relative motion accurately. Because the cross-beat frequency between the particles across two measuring regions is shifted to a frequency ($\Omega = 40$ MHz) much higher than the self-beat frequency, we can easily pick up the cross-beat signals by using a bandpass filter. The optical

mixing at the high frequency also discriminates all sorts of low-frequency electronic noise, making the technique particularly useful for samples with small MSRD. By using the best digital correlator available in the market, we can have a temporal resolution in many decades of a time span down to 50 ns. The fast digital correlator also allows us to measure $g(\tau)$ in real time. As a result, the dual-beam micro-DLS offers wider frequency range, higher accuracy, and better averaging compared with the video-based MPT methods. It is a local probe and requires a small sample volume. Measurements of the relative motion of the particles in a rheologically inhomogeneous sample, such as a live cell, can be carried out by a scan of the laser beams over an area of interest. This can be accomplished readily by use of the fine scanning capability of the microscope stage.

6. Summary

We have devised a dual-beam DLS scheme to measure the MSRD, $\langle \Delta \mathbf{r}_{21}{}^2(l, \tau) \rangle$, of tracer particle pairs. With two parallel laser beams, the new technique measures the cross-beat signals between two tracer particles across the two incident laser beams. Because it is based on the same optical beating principle, the dual-beam DLS works in a way similar to the standard one-beam DLS. The only difference is that the beat signals in the dual-beam scheme result from particle pairs across two different scattering regions with a small separation l (cross-beat). In the standard one-beam DLS, however, the signals come from the beating of the individual particles in the same scattering volume (self-beat).

To find optimal experimental conditions for the dual-beam DLS, we measure the relative diffusion of uniform latex spheres suspended in a simple viscous fluid. The experiment verifies the working principle of the dual-beam DLS and demonstrates its applications. It is found that the dual-beam DLS measures MSRD with the same high accuracy and high statistical averaging as the one-beam DLS does for the MSD of individual tracer particles. To obtain the highest spatial resolution and the best optical alignment, we devise a new optical arrangement to carry out the dual-beam DLS on an inverted optical microscope (referred to as micro-DLS). Micro-DLS will have wide use in the general area of soft condensed-matter physics, especially in the study of two-particle microrheology of complex fluids and biomaterials.

From the definition of MSRD, we have $\langle \Delta \mathbf{r}_{21}{}^2(l, \tau) \rangle = 2\langle \Delta \mathbf{r}_i{}^2 \rangle_t - 2\langle \Delta \mathbf{r}_2 \cdot \Delta \mathbf{r}_1 \rangle_t$, where $\langle \Delta \mathbf{r}_i{}^2 \rangle_t$ is the single-particle MSD, which changes with the particle radius but is independent of the particle separation l. The cross-diffusion term $\langle \Delta \mathbf{r}_2 \cdot \Delta \mathbf{r}_1 \rangle_t$ depends on both l and the delay time τ. In two-particle microrheology, we are actually interested in the τ dependence of $\langle \Delta \mathbf{r}_2 \cdot \Delta \mathbf{r}_1 \rangle_t$, which is related to the complex shear modulus $G^*(\omega)$ by the GSER.[13] Because the self-diffusion term contributes only a multiplicative factor $\exp[-q^2 \langle \Delta \mathbf{r}_i{}^2 \rangle_t]$ to the intensity correlation function $G_{12}(\tau)$, its effect can be readily divided out from the measured $G_{12}(\tau)$. We do this by measuring the single-particle correlation function $\exp[-q^2 \langle \Delta \mathbf{r}_i{}^2 \rangle_t]$ independently by using the same experimental setup but with only one beam present in the scattering volume. The corrected $G_{12}(\tau)$, which is proportional to $\exp[q^2 \langle \Delta \mathbf{r}_2 \cdot \Delta \mathbf{r}_1 \rangle_t]$, thus becomes the basic function for optical two-particle microrheology.

The new technique of micro-DLS should be compared with the video-based MPT methods, which have been used increasingly in recent years.[6–9] With the aid of video microscopy, MPT follows the motions of several hundreds of micrometer-sized particles in each frame of a video simultaneously and obtains the ensemble average $\langle \Delta \mathbf{r}_2 \cdot \Delta \mathbf{r}_1 \rangle_t$ or MSD from each of the individual particle trajectories. The ability to uniquely identify each particle in each frame of a video and accurately determine the center of the two-dimensional particle images is critical to the method. MPT requires postprocessing of the video images by sophisticated image-analysis programs, and therefore $\langle \Delta \mathbf{r}_2 \cdot \Delta \mathbf{r}_1 \rangle_t$ cannot be obtained in real time. The frequency range of the measured $\langle \Delta \mathbf{r}_2 \cdot \Delta \mathbf{r}_1 \rangle_t$ is limited by the frame rate of the camera (typically, 15–30 frames/s). Because the relative displacement between two particles is obtained through the subtraction of the particle positions, the measured $\langle \Delta \mathbf{r}_2 \cdot \Delta \mathbf{r}_1 \rangle_t$ becomes sensitive to the background noise, such as that from sample vibration and velocity drifts.

Micro-DLS, on the other hand, is a local probe, which measures $\langle \Delta \mathbf{r}_{21}{}^2(l, \tau) \rangle$ (and hence $\langle \Delta \mathbf{r}_2 \cdot \Delta \mathbf{r}_1 \rangle_t$) at a point of size 1–10 μm. Measurements of $\langle \Delta \mathbf{r}_{21}{}^2(l, \tau) \rangle$ in a rheologically inhomogeneous sample is carried out by a scan of the probe over an area of interest. By use of two parallel incident laser beams of different frequencies, the technique picks up the scattering signals from the particle pairs across the two incident beams and measures $\langle \Delta \mathbf{r}_{21}{}^2(l, \tau) \rangle$ directly and precisely by means of optical mixing. With a fast digital correlator, we can measure the intensity autocorrelation function $g(\tau)$ in real time and obtain $\langle \Delta \mathbf{r}_{21}{}^2(l, \tau) \rangle$ over a time span from hours to 50 ns. Photon correlation spectroscopy is a mature technology that provides excellent sample averaging and is easy to use. Consequently, micro-DLS offers a wider frequency range, higher accuracy, and better averaging compared with MPT. Its ability of measuring $\langle \Delta \mathbf{r}_{21}{}^2(l, \tau) \rangle$ in real time and the precise optics and fast electronics available for photon correlation spectroscopy make micro-DLS a particularly useful and convenient tool for the experimental study of two-particle microrheology of soft materials.

We thank D. A. Weitz and X. R. Wang for useful discussions. The assistance of M. Lucas and his team in fabricating the experimental apparatus is gratefully acknowledged. This work was supported by the National Science Foundation under grant DMR-0071323. P. Tong was also supported in part by the Research Grants Council of Hong Kong SAR under grant HKUST 603003.

References

1. B. J. Berne and R. Pecora, *Dynamic Light Scattering* (Wiley, New York, 1976).
2. T. G. Mason and D. A. Weitz, "Optical measurements of frequency-dependent linear viscoelastic moduli of complex fluids," Phys. Rev. Lett. **74,** 1250–1253 (1995).
3. T. G. Mason, K. Ganesan, J. H. van Zanten, D. Wirtz, and S. C. Kuo, "Particle tracking microrheology of complex fluids," Phys. Rev. Lett. **79,** 3282–3285 (1997).
4. A. J. Levine and T. C. Lubensky, "One- and two-particle microrheology," Phys. Rev. Lett. **85,** 1774–1777 (2000).
5. A. J. Levine and T. C. Lubensky, "Two-point microrheology and the electrostatic analogy," Phys. Rev. E **65,** 011501 (2001).
6. T. Gisler and D. A. Weitz, "Tracer microrheology in complex fluids," Curr. Opin. Colloid Interface Sci. **3,** 586–592 (1998).
7. F. C. MacKintosh and C. F. Schmidt, "Microrheology," Curr. Opin. Colloid Interface Sci. **4,** 300–307 (1999).
8. M. L. Gardel, M. T. Valentine, and D. A. Weitz, "Microrheology," in *Microscale Diagnostic Techniques*, K. Breuer, ed. (Springer-Verlag, New York, to be published).
9. Y. Tseng, T. P. Kole, S.-H. J. Lee, and D. Wirtz, "Local dynamics and viscoelastic properties of cell biological systems," Curr. Opin. Colloid Interface Sci. **7,** 210–217 (2002).
10. J.-C. Meiners and S. R. Quake, "Direct measurement of hydrodynamic cross correlations between two particles in an external potential," Phys. Rev. Lett. **82,** 2211–2214 (1999).
11. Y. Tseng, T. P. Kole, and D. Wirtz, "Micromechanical mapping of live cells by multiple-particle-tracking microrheology," Biophys. J. **83,** 3162–3176 (2002).
12. X. Ye, P. Tong, and L. J. Fetters, "Transport of probe particles in semidilute polymer solutions," Macromolecules **31,** 5785–5793 (1998).
13. J. C. Crocker, M. T. Valentine, E. R. Weeks, T. Gisler, P. D. Kaplan, A. G. Yodh, and D. A. Weitz, "Two-point microrheology of inhomogeneous soft materials," Phys. Rev. Lett. **85,** 888–891 (2000).
14. J. C. Crocker and D. G. Grier, "Methods of digital video microscopy," J. Colloid Interface Sci. **179,** 298–310 (1996).
15. H. Z. Cummins and H. L. Swinney, "Light beating spectroscopy," in *Progress in Optics, Vol. VIII*, E. Wolf, ed. (Elsevier North-Holland, Amsterdam, 1970).
16. E. R. Dufresne, T. M. Squires, M. P. Brenner, and D. G. Grier, "Hydrodynamic coupling of two Brownian spheres to a planar surface," Phys. Rev. Lett. **85,** 3317–3320 (2000).
17. D. L. Ermak and J. A. Mecammon, "Brownian dynamics with hydrodynamic interactions," J. Chem. Phys. **69,** 1352–1360 (1978).
18. G. K. Batchelor, "Brownian diffusion of particles with hydrodynamic interaction," J. Fluid Mech. **74,** 1–29 (1976).
19. J. C. Crocker, "Measurement of the hydrodynamic corrections to the Brownian motion of two colloidal particles," J. Chem. Phys. **106,** 2837–2840 (1997).
20. T. Narayanan, C. Cheung, P. Tong, W. I. Goldburg, and X.-L. Wu, "Measurement of the velocity difference by photon correlation spectroscopy: an improved scheme," Appl. Opt. **36,** 7639–7644 (1997).
21. Y.-X. Du, B. J. Ackerson, and P. Tong, "Velocity difference measurement with a fiber-optic coupler," J. Opt. Soc. Am. A **15,** 2433–2439 (1998).
22. P. D. Kaplan, V. Trappe, and D. A. Weitz, "Light-scattering microscope," Appl. Opt. **38,** 4151–4157 (1999).
23. E. J. Hinch and L. C. Nitsche, "Non-linear drift interactions between fluctuating colloidal particles: oscillatory and stochastic motions," J. Fluid Mech. **256,** 343–401 (1993).
24. M. T. Valentine, A. K. Popp, D. A. Weitz, and P. D. Kaplan, "Microscope-based static light-scattering instrument," Opt. Lett. **26,** 890–892 (2001).